scientific reports

Check for updates

OPEN

Exploring the protective role of caffeine against *Taraxacum*-Induced ribotoxic stress mediated through autophagy and mitochondrial depolarization

Chien-Jung Lin[1], Shu-Ting Liu[2], Zih-Syuan Wu[2,3], Shih-Ming Huang[2] & Teng-Wei Chen[4]✉

The ribotoxic stress response is a pathway that gets activated when ribosomes get impaired, leading to disruptions in protein synthesis, increased inflammatory signaling, and cell death if left unresolved. *Taraxacum* can induce apoptosis-associated ribosomal RNA (rRNA) cleavage, however, the exact working mechanism of *Taraxacum*-induced rRNA cleavage remains unclear. In this study, we used the RNA integrity (RIN) value and 28S/18S ratio to confirm the integrity of experiments. Our RNA sequencing data showed that *Taraxacum formosanum* (*T. formosanum*) upregulated 893 genes and downregulated 509 genes and triggered hallmark genes of spliceosomes, TNF-α signaling via NF-κB, inflammatory response, and IL6-JAK-STAT3 signaling. Additionally, *T. formosanum* imbalanced the levels of ribosomal proteins of the large and small subunits. We found that caffeine was the only screening agent that could rescue the cleavage of 28S and 18S rRNA induced by *T. formosanum*. However, caffeine failed to rescue *T. formosanum*-targeted mRNAs when the RIN values were relatively lower. *T. formosanum* induced the N-terminal clipping of histone H3, which was observed not only in human HeLa cervical cancer cells but also in human Huh6 and HepG2 liver cancer cells. Our study revealed that caffeine could reverse the effects of *T. formosanum* on the reduction of autophagy and the disruption of mitochondrial membrane potential. However, caffeine could only change the populations of necrotic and apoptotic cells but not *T. formosanum*-induced cell death. By providing detailed information on *Taraxacum*-induced rRNA cleavage and N-truncated histone H3's mechanisms of gene regulation, we hope to understand their respective cellular death and survival stresses.

Keywords Ribotoxic stress response, Ribosomal RNA cleavage, H3 N-tail cleavage, *Taraxacum formosanum*, Mitochondrial depolarization

The term 'ribotoxic stress response (RSR)' was coined in 1997 by Iordanov et al.. The researchers demonstrated that drugs and toxins that interfere with the region of 28S ribosomal RNA (rRNA) critical for amino acid-tRNA binding, peptidyl transfer, and translocation, activate p38 and JNK, which are stress- and mitogen-activated protein (MAP) kinases[1]. The RSR is one such pathway that is activated by ribosomal impairment, which can disrupt protein synthesis, increase inflammatory signaling, and even lead to cell death if left unresolved[2]. The RSR has an important physiological role in regulating cell-fate decisions, cytokine expression, and balancing apoptosis and cell survival during immune responses[3–6]. RSR triggers have been identified, including translation inhibitors, ribotoxins, chemotherapeutics, and UV radiation. These agents cause structural damage to rRNA, impair ribosome function, and lead to the strong activation of p38 and JNK. The initial signaling triggers a proinflammatory response, but if the duration or magnitude of RSR signaling is sufficient, it can eventually lead to cell death. In addition to the RSR, there are two other main translation surveillance pathways, Ribosome-

[1]Department of Chinese Medicine, Tri-Service General Hospital, National Defense Medical Center, Taipei City 114, Taiwan, Republic of China. [2]Department of Biochemistry, National Defense Medical Center, Taipei City 114, Taiwan, Republic of China. [3]Institute of Life Sciences, National Defense Medical Center, Taipei City 114, Taiwan, Republic of China. [4]Division of General Surgery, Department of Surgery, Tri-Service General Hospital, National Defense Medical Center, Taipei City 114, Taiwan, Republic of China. ✉email: DOC20264@mail.ndmctsgh.edu.tw

associated Quality Control and Integrated Stress Response, which also play important roles in maintaining cellular homeostasis.

RNA degradation is a crucial process in gene expression regulation that controls coding and non-coding RNA levels in response to developmental and environmental cues[7,8]. It also plays a vital role in eliminating defective RNAs that can be produced during the maturation of functional transcripts from their precursors. The control of RNA quality prevents the accumulation of aberrant non-coding transcripts or the translation of defective messenger RNAs (mRNAs), which could potentially cause deleterious effects. Studies have shown that RNA degradation can prompt death execution, as malfunction of the protein synthesis machinery may occur following rRNA degradation[9]. Viral and endogenous double-stranded RNA (dsRNA) can also trigger programmed RNA degradation by the 2–5 A/RNase L complex, termed 2-5AMD. This response switches global protein synthesis from homeostasis to production of interferons[10]. RNase L cleaves a broad spectrum of host RNAs, including rRNAs, tRNAs, mRNAs, and Y-RNAs. Although the cleavage of rRNA does not inhibit the activity of the ribosome, recent studies have shown that mRNA levels in the cell can be reduced up to ~90% due to RNase L, causing a global effect termed 2-5AMD[10,11]. Interestingly, mRNA decay fragments via the nonsense mediated decay (NMD)[12], may be translated to produce short peptides that could be important for antiviral activity or others[13].

The histone H3 N-terminal protein domain, also known as N-tail, is subject to regulation through various posttranslational modifications such as methylation, acetylation, phosphorylation, and proteolytic cleavage[14]. Cleavage is observed to be more frequent at gene promoters that are bound and repressed by JMJD5, which suggests that H3 N-tail cleavage plays a role in gene expression regulation[15]. There have been many studies demonstrating the importance of histone H3 clipping in various biological processes, such as human embryonic stem cell lines (ESCs) and human peripheral blood mononuclear cells (PBMCs), regulation of monocyte-to-macrophage differentiation, a novel signature of human neutrophil extracellular traps, and regulation of myoblast differentiation[15–19]. In addition to the well-known cysteine protease Cathepsin L[19], glutamate dehydrogenase and MMP-2 have been identified as novel H3 N-tail proteases[20,21]. These proteases primarily cleave at amino acid residue A21, but multiple other sites have also been found at amino acid residues: T22, K23, A24, R26, and K27 [17]. The potential effects of histone tail clipping may lead to altered electrostatic interactions between histones and DNA and remove existing histone marks, either activating or repressive, which may erase epigenetic memory and alter the regulation of cell-type-specific gene transcription.

For centuries, in traditional medicine, *Taraxacum*reportedly exhibited analgesic, angiogenic, anti-allergic, anticarcinogen, anticoagulant, anti-inflammatory, antirheumatic, antioxidant, cholagogue, choleretic, and diuretic properties, among others[22–26]. *Taraxacum*-induced cell death could be due to the cleavage of 28S rRNA. This cleavage may lead to apoptosis-associated rRNA cleavage and activate signals such as JNK, p38, and RPS6 [27]. It is possible that *Taraxacum*-induced 28S rRNA cleavage may have similar biological consequences to an RSR, such as apoptosis. In a previous study, we investigated the potential antitumor effects of aqueous extracts from two species of *Taraxacum*, *T. mongolicum* and *T. formosanum*, on HeLa human cervical cancer cells and various types of liver cancer cells[27]. Our results showed that the extracts suppressed cellular proliferation and transcription while inducing necrosis, late apoptosis, and endoplasmic reticulum (ER) stress in HeLa cells. Another study focused on the potential antitumor effects of these species on three human breast cancer cell lines: the MDA-MB-231 TNBC cell line, and the ZR75-1 and MCF-7 hormone-dependent breast cancer cell lines[28]. The study found that *T. mongolicum* exhibited cytotoxic effects against MDA-MB-231 cells, including the induction of apoptosis, suppression of cellular proliferation, colony formation, migration, disruption of the mitochondrial membrane potential, and downregulation of the oxygen consumption rate. In contrast, *T. formosanum* induced ribotoxic stress in MDA-MB-231 and ZR-75-1 cells, while *T. mongolicum* did not.

Mitochondrial depolarization occurs when there is a loss of mitochondrial membrane potential, which is often linked to impaired mitochondrial function. This disruption can result in cellular dysfunction and may eventually lead to cell death[29]. Autophagy is a cellular survival pathway that helps cells compensate for nutrient depletion and ensures the appropriate degradation of organelles[30]. Mitophagy is a related process that regulates mitochondrial number and health by subjecting excessive or damaged mitochondria to autophagic degradation[31]. Evidence suggests that mitochondria can also significantly influence the autophagic process[32]. Mitophagic malfunction can lead to the accumulation of dysfunctional mitochondria, making the cell more susceptible to mitochondrial membrane permeabilization and apoptosis. In turn, apoptotic executers can inactivate pro-autophagic proteins, inhibiting autophagy and leading to cell death[33]. In this study, we aimed to address three important issues related to the effect of *Taraxacum* on the quality of 28S rRNA, such as cleaved rRNA fragments, affects the stability of mRNAs or/and protein synthesis, and then to identify the rescue reagents. We tried to elucidate whether the working mechanisms of RSR, rRNA cleavage, and histone H3 N-tail clipping have linked each other or related to each other. With the detailed information obtained from our study, we hope to elucidate the mechanisms of gene regulation from cleaved rRNAs and N-truncated histone H3 to mRNAs, and their respective cellular death and survival stresses.

Results

The verification of the cleavage of rRNAs and the ribotoxic stress response by *T. formosanum* via the RIN value and RNA sequencing analysis in human cervical HeLa cells

The integrity of RNA molecules is of paramount importance for experiments that try to reflect the snapshot of gene expression at the moment of RNA extraction. The advent of microcapillary electrophoretic RNA separation provides the basis for an automated high-throughput approach, in order to estimate the integrity of RNA (RIN) samples in an unambiguous way with an Agilent 2100 bioanalyzer[34]. RIN values range from 10 (intact) to 1 (totally degraded) based on adaptive learning tools. The data of microcapillary electropherogram are divided into different areas and peaks, and the analysis software supporting the Agilent 2100 bioanalyzer can generate

RIN values and 28S/18S ratios based on the test results. Our previous results showed that rRNA degradation could be detected with RNA agarose gel electrophoresis[27]. We applied microcapillary electrophoretic RNA separation to calculate RIN values and 28S/18S ratios of *T. formosanum* and *T. mongolicum* treated HeLa cells. We compared the general RNA agarose gel electrophoresis (Fig. 1A) and microcapillary electrophoretic RNA separation (Fig. 1B) in *T. formosanum* treated HeLa cells. The red single- and double-arrow in Fig. 1A indicate cleaved 28S rRNA and 18S rRNA, while the red single- and double-arrow in Fig. 1B indicate intact 28S rRNA and 18S rRNA. We observed the cleavage of 28S rRNA and 18S rRNA when the concentrations of *T. formosanum* and *T. mongolicum* were over 7 mg/mL. We calculated the ratio of 28S/18S and RIN value for individual *T. formosanum* concentration (Fig. 1C). The ratio of 28S/18S decreased from 2.1 to 0.1, and the value of RIN decreased from 8.5 to 5.0. These data suggest that the quality of rRNAs was disrupted by *T. formosanum* and *T. mongolicum* extract-treated HeLa cells. Our current data support that *T. formosanum* extract might have the ability to degrade 28S rRNA and 18S rRNA in HeLa cells via the reliable microcapillary electrophoretic RNA separation plus RIN value.

Higher amounts of *T. mongolicum* and *T. formosanum*-induced rRNA degradation had been found to suppress most mRNAs, including well-known internal mRNA control *GAPDH* and *β-actin*, while their proteins were

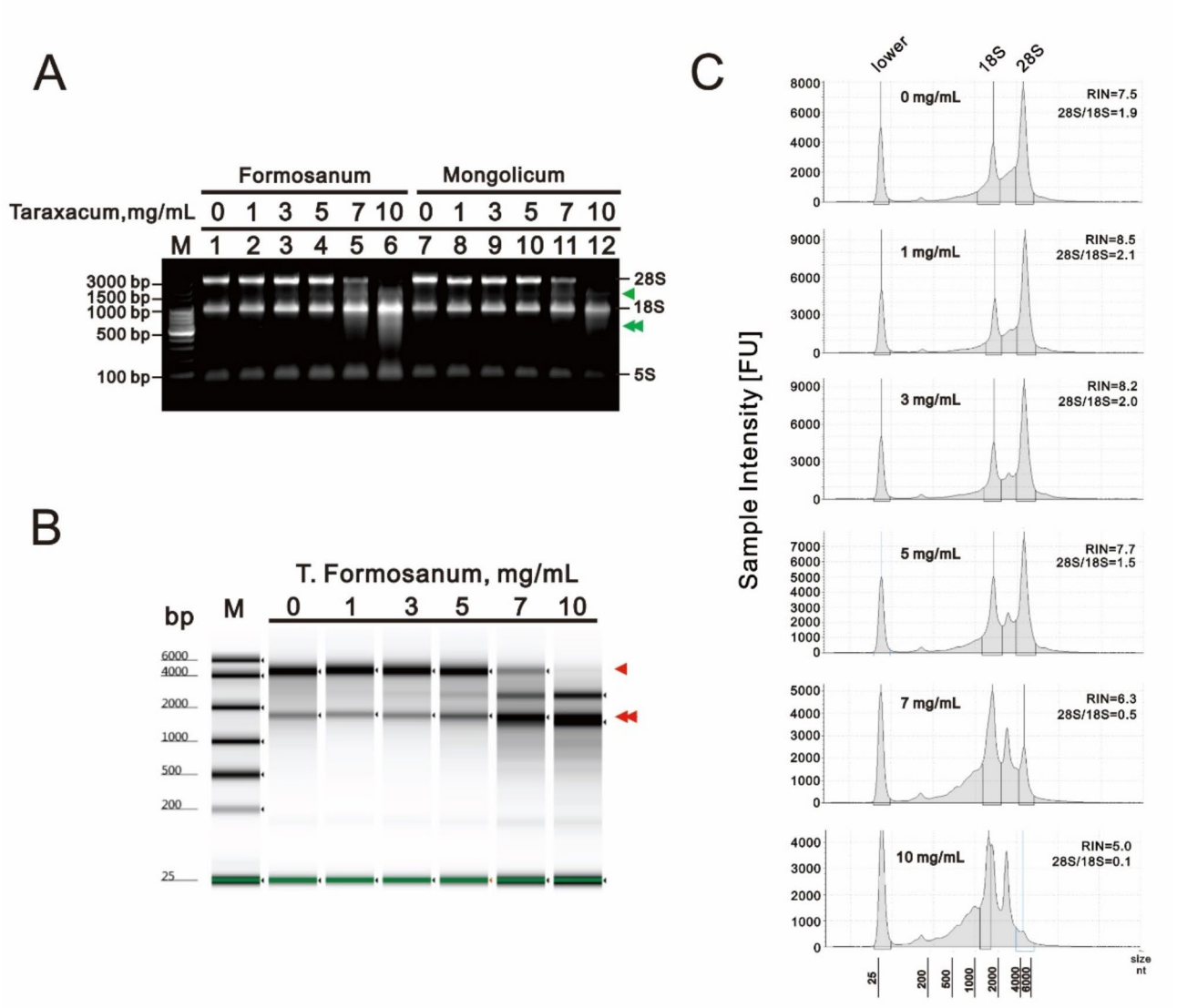

Fig. 1. Effects of *T. formosanum* and *T. mongolicum* on the RNA quality in HeLa cells. (**A**-**C**) HeLa cells were treated for 24 h with the indicated concentrations of *T. mongolicum* or *T. formosanum*, after which their cell lysates were subjected to (**A**) total RNA agarose gel electrophoresis analysis; (**B**) total RNA microcapillary electrophoresis analysis; (**C**) microcapillary electropherograms were generated by Agilent 2100 bioanalyzer. The green single-arrow is the cleaved 28S rRNA and the double-arrow is the cleaved 18S rRNA. The red single-arrow is 28S rRNA and the double-arrow is 18S rRNA for the measure of RIN value. M, bp: the molecular weight of rRNA.

expressed well in HeLa cells[27]. To further understand the relationship between rRNA degradation and mRNA stability, lower amounts of *T. mongolicum* or *T. formosanum* were combined with *de novo* mRNA synthesis inhibitor actinomycin D (Act D) in HeLa cells to analyze mRNA stability. Using the total RNA agarose gel analysis, there was no apparent difference in each group (Fig. 2A). However, during the 4-hour window with Act D treatment, through RT-PCR analysis of target mRNA expression, we detected a reduction in the abundance of stable mRNAs, including *p21*, *C/EBP-homologous protein* (*CHOP*), and *interleukin-6* (*IL-6*) (Fig. 2B, compared with lanes 1, 5, and 9). However, the treatment of HeLa cells with *T. mongolicum* and *T. formosanum* induced the expression of *p21*, *CHOP*, and *IL-6* mRNA. In the western blotting analysis (Fig. 2C), we found that hypoxia-inducible factor 1 alpha (HIF-1α) protein might suppress *cyclin B1* mRNA as a repressor and induce *CHOP*mRNA as an activator based on previous literature[35,36]. Additionally, histone H3 chipping fragments were induced by *T. mongolicum* and *T. formosanum*, and the changes of H3P (phosphorylation of histone H3 serine 10) and demethylation of histone H3 lysine 79, H3(K79), proteins. Our data showed that the signals of H3P were suppressed with the increasing amounts of *T. mongolicum* and *T. formosanum*, but the signals of dimethyl H3(K79) were not affected. However, we need the optimal condition of *T. mongolicum* and *T. formosanum* to elucidate their effects on the stability of some mRNAs, including internal mRNA control *GAPDH*.

It has been demonstrated that certain agents inducing structural damage to rRNA and impair ribosome function can trigger a robust activation of a proinflammatory response[3–6]. In this study, we applied RNA sequencing analysis to compare *T. formosanum* extract-treated HeLa cells in terms of gene expression. The analysis revealed 893 upregulated genes and 509 downregulated genes (Fig. 3A). Among the highlighted upregulated genes were small nuclear RNAs (snRNAs). Most snRNAs are involved in the splicing of introns

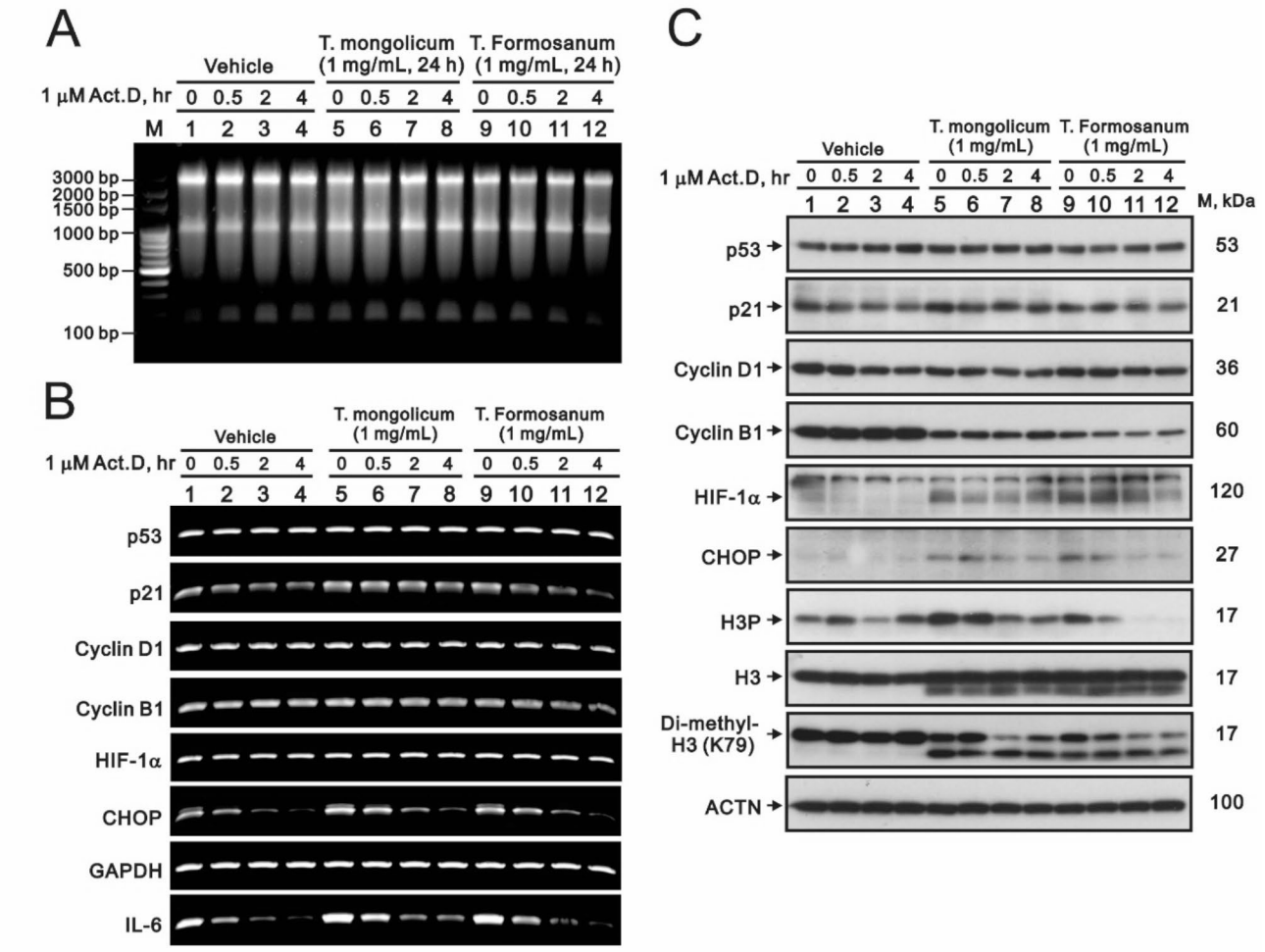

Fig. 2. Effects of *T. mongolicum* and *T. formosanum* on rRNAs, mRNAs, and proteins in HeLa cells. (**A-C**) HeLa cells were treated for 24 h with the indicated concentrations of *T. mongolicum* or *T. formosanum* in the presence of various time of 1μM Act D treatment, after which their cell lysates were subjected to (**A**) total RNA agarose gel electrophoresis analysis; (**B**) RT-PCR analysis using primer pairs against the indicated mRNAs, with *GAPDH* mRNA as the mRNA loading and internal control; (**C**) western blot analysis using antibodies against the indicated proteins, with ACTN as the protein loading control (supplementary file 1). M, bp: the molecular weight of rRNA. M, kDa: the molecular weight of protein.

from pre-mRNA as part of either the major or minor spliceosome[8]. The major spliceosome features U1, U2, U4, U5, and U6 snRNPs. U1 snRNP protects pre-mRNAs from premature cleavage and polyadenylation[37]. All snRNA genes are named with the root symbol "RNU" for "RNA, U# small nuclear." In this study, two highlighted downregulated genes were POLR2A and RNU6ATAC35P. The POLR2A gene encodes the largest subunit of RNA polymerase II, while RNU6ATAC35P is a small RNA molecule found in the cell nucleus that is involved in the processing of pre-mRNA snRNA. It is worth noting that human spliceosomal snRNA sequence variants generate variant spliceosomes[38]. One of the most conserved mechanisms by which cells sense viral infection is through the detection of dsRNAs by a set of receptors in the innate immune system that trigger antiviral and inflammatory immune responses[39]. Gene set enrichment analysis (GSEA) by *T. formosanum* showed that hallmark TNF-α signaling via NF-κB, Inflammatory response, and IL6-JAK-STAT3 signaling were all affected (Fig. 3B).

The rescuing mechanisms of caffeine for the cleavage of rRNAs by *T. formosanum* in human cervical HeLa cells

We utilized various inhibitors to rescue the 28S rRNA cleavage induced by 5 mg/mL *T. formosanum* for 24 h, 10 mg/mL *T. formosanum* for 8 h, and 7 mg/mL *T. formosanum* for 16 h, including signaling kinase inhibitors (such as p38 kinase inhibitor SB203580, MAPK inhibitor PD98059, AKT/PI3K inhibitor LY294002, JNK inhibitor, ribosomal S6K inhibitor BI-D1870, and EGFR tyrosine kinase inhibitor AG1478), antioxidant ellagic acid, de novo mRNA synthesis inhibitor Act D, proteasome inhibitor MG132, lysosome inhibitor ammonium chloride (NH_4Cl), p53 transcription activity inhibitor PFT-α, apoptosis inhibitor Z-VAD-FMK, calpain inhibitor

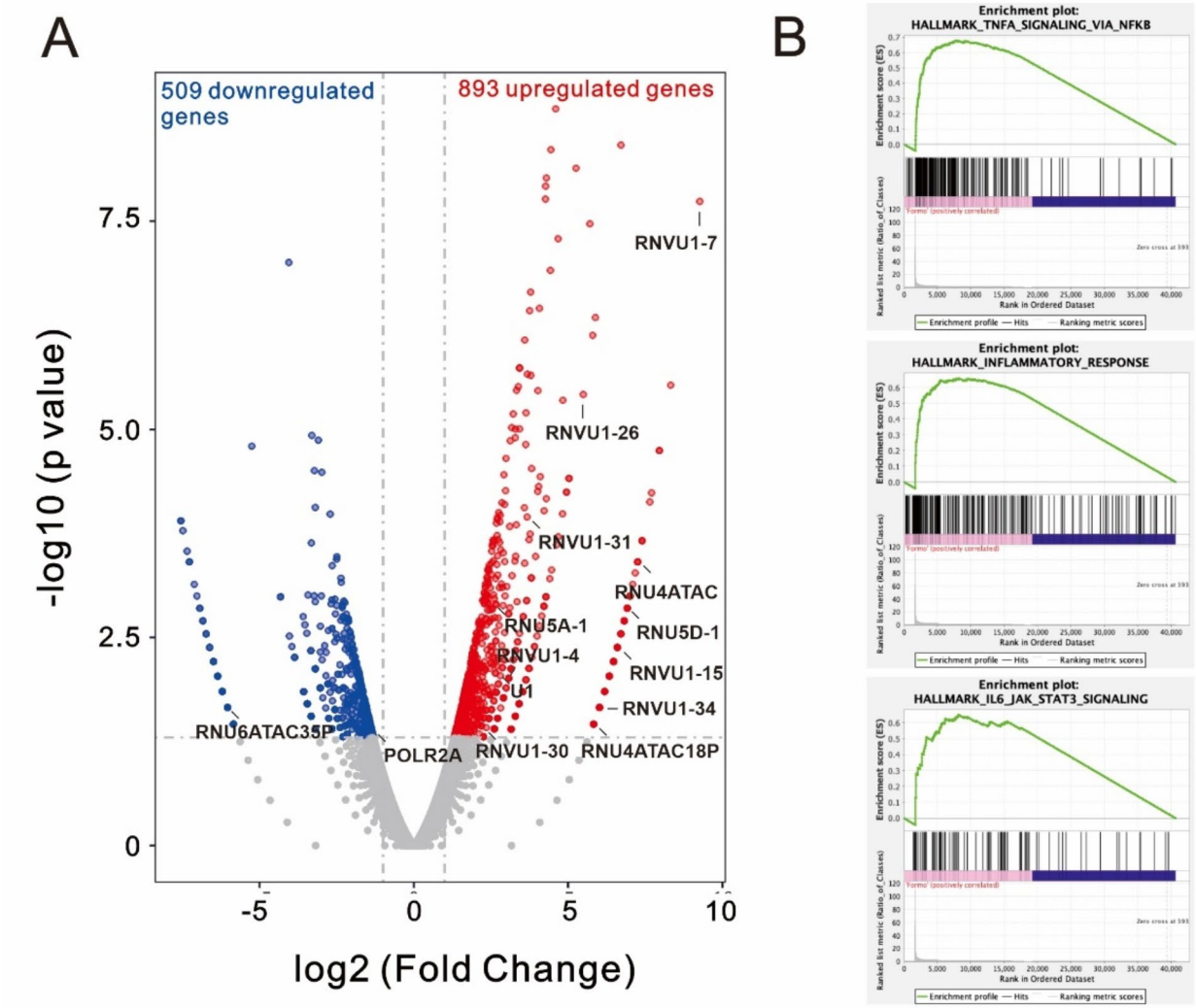

Fig. 3. The RNA sequencing analysis of *T. formosanum* extract-treated HeLa cells. (**A**) Volcano plot and highlighted up- and down-regulated genes. (**B**) Gene set enrichment analysis for TNF-α signaling via NF-κB, Inflammatory response, and IL6-JAK-STAT3 signaling.

II ALLM, adenosine receptor antagonist caffeine, Na^+/K^+ ATPase ligand ouabain, and anti-inflammatory agent resveratrol (Fig. 4A-D). Our data suggest that caffeine might be one of the choices for rescuing the 28S and 18S rRNA cleavage induced by *T. formosanum* in HeLa cells.

We further elucidated the rescue mechanisms of caffeine in *T. formosanum* extract-treated HeLa cells. The RNA quality index and 28S/18S ratio decreased RIN value from 7.8 to 4.8 and 28S/18S ratio from 1.4 to 0.3 by *T. formosanum* (Fig. 5A). However, caffeine restored both RIN and the 28S/18S ratio to 6.3 and 0.4, respectively. The total RNA agarose gel electrophoresis also revealed alterations in 28S and 18S rRNA fragments induced by *T. formosanum*, and these changes were reversed in the presence of caffeine (Fig. 5B). However, the RT-PCR data exhibited patterns consistent with those presented in our previous publication[27], indicating that several target mRNAs, including *GAPDH* and *β-actin*, were challenging to detect in the presence of *T. formosanum* (Fig. 5C). In this suppression of *T. formosanum*, caffeine appeared to be ineffective in rescuing any mRNA. Notably, we observed interesting data in the western blotting analysis (Fig. 5D). The effects of *T. formosanum*on cyclin D1, HIF-1α, and histone H3 clipping fragments were reversed with the addition of caffeine. Moreover, we observed consistent findings regarding the specific effects of caffeine on p53 and cleaved PARP proteins with our previous publication[27].

Based on the defect of rRNAs, we analyzed the effects of *T. formosanum* on ribosomal proteins, including ribosomal proteins of large subunit and small subunit (RPLs and RPSs) using the RNA sequencing data. We summarized up- and down-regulated *RPLs* and *RPSs* by *T. formosanum* and rescued by caffeine (Fig. 6A). We then selected some *RPLs* (*RPL3*, *RPL4*, and *RPL6*) and *RPSs* (*RPS2* and *RPS26*) for the verification of the rescue effect of caffeine with PCR gel agarose electrophoresis (Fig. 6B). Most of them were consistent with the analysis of RNA sequencing data.

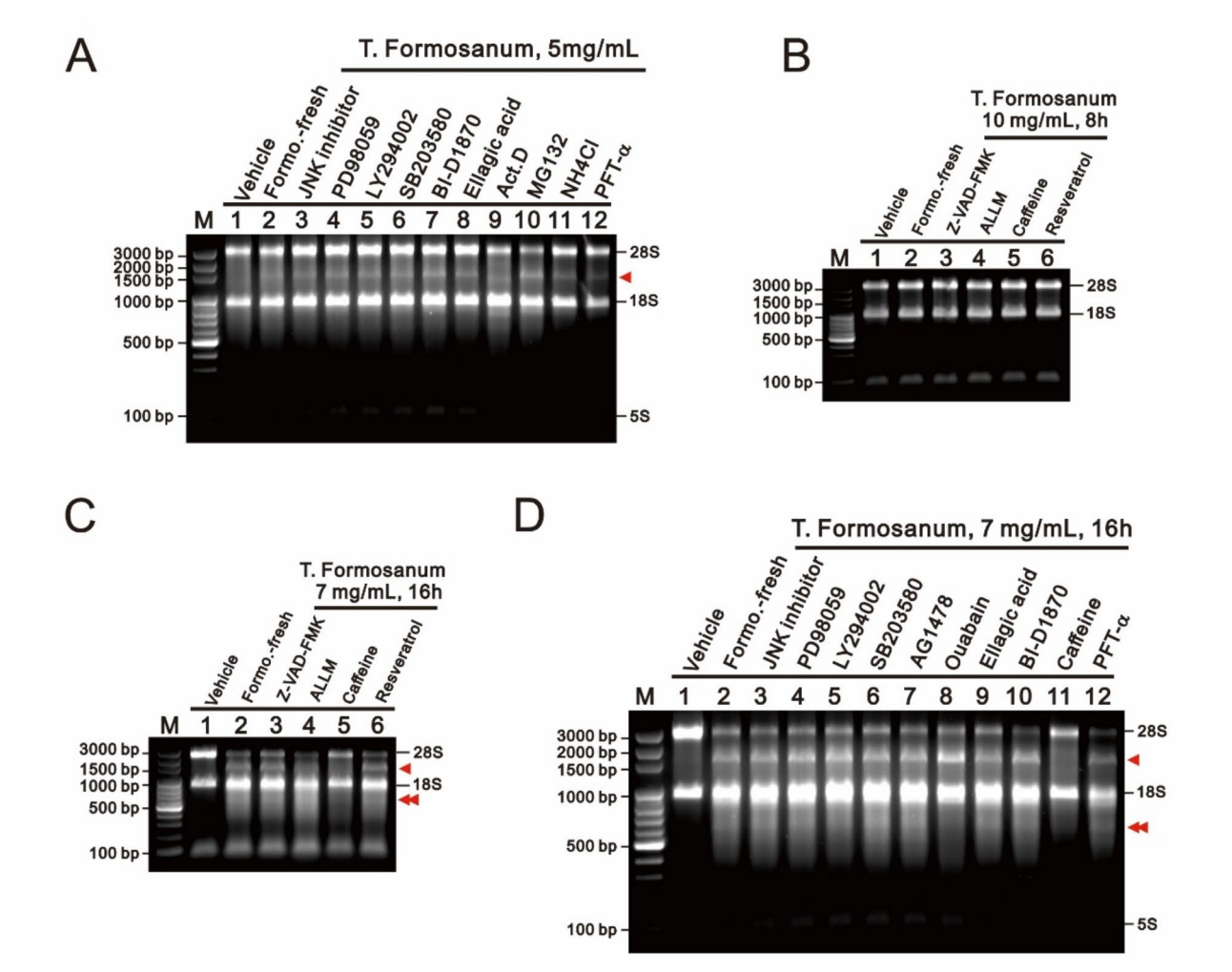

Fig. 4. The drug screening procedure was to rescue the cleavage of 18S and 28S rRNA by *T. formosanum* in HeLa cells. (**A-D**) HeLa cells were treated for the indicated concentrations of *T. formosanum* and various potential drugs treated with indicated time, after which their cell lysates were subjected to total RNA agarose gel electrophoresis analysis. The red single-arrow is the cleaved 28S rRNA and the double-arrow is the cleaved 18S rRNA. M, bp: the molecular weight of rRNA.

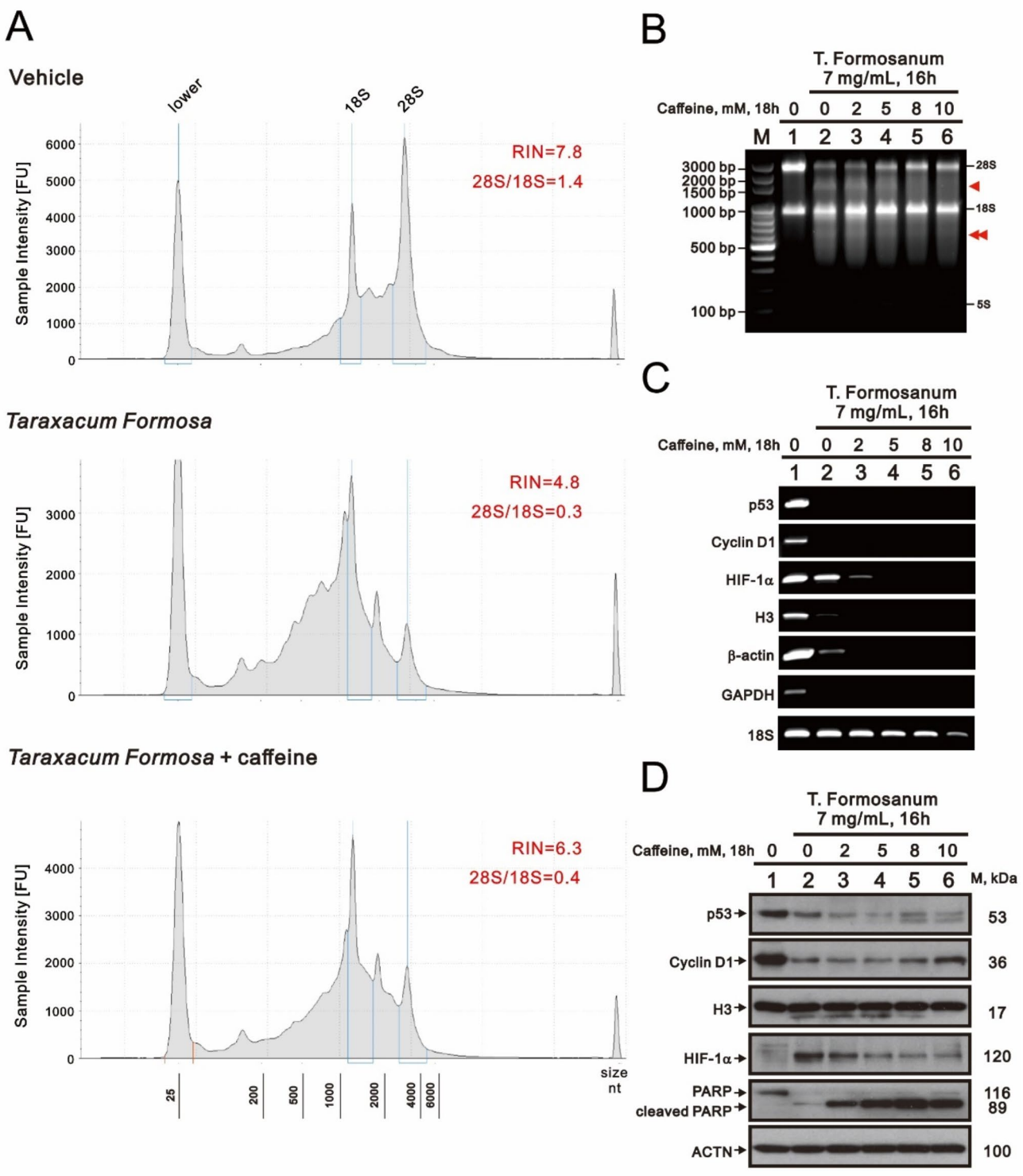

Fig. 5. The rescue effects of caffeine on the *T. formosanum*-induced 18S and 28S rRNAs cleavage in HeLa cells. (**A-D**) HeLa cells were treated with 7 mg/mL *T. formosanum* for 16 h alone or in the presence of pretreated with indicated amounts of caffeine for 2 h, after which their cell lysates were subjected to (**A**) total RNA microcapillary electrophoresis analysis and microcapillary electropherograms were generated by Agilent 2100 bioanalyzer. (**B**) total RNA agarose gel electrophoresis analysis; (**C**) RT-PCR analysis using primer pairs against the indicated mRNAs, with *GAPDH* mRNA as the mRNA loading control and 18S rRNA as an internal control; (**D**) western blot analysis using antibodies against the indicated proteins, with ACTN as the protein loading control. M, bp: the molecular weight of rRNA. M, kDa: the molecular weight of protein.

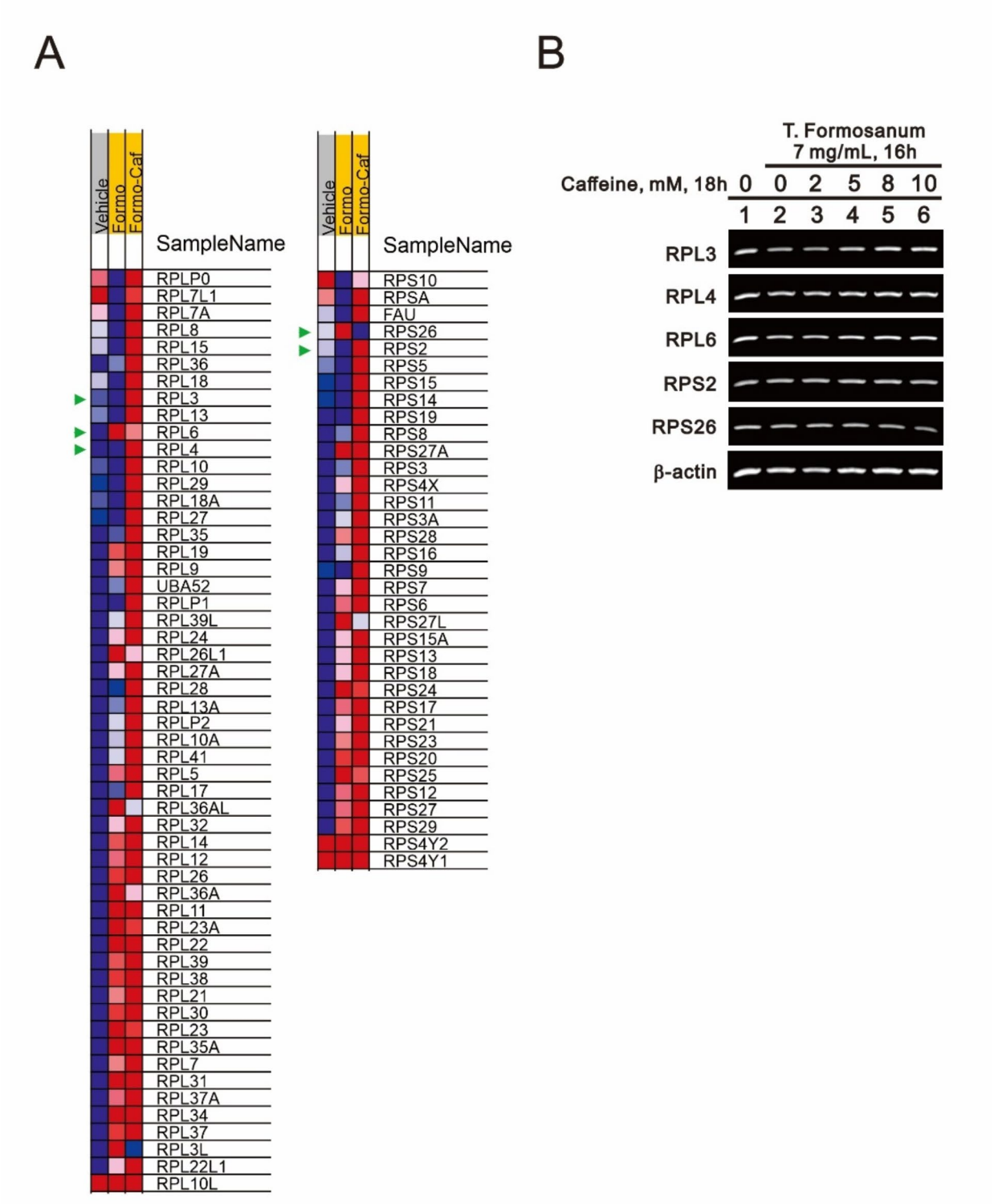

Fig. 6. Effects of *T. formosanum* on ribosomal protein genes in HeLa cells. (**A** and **B**) HeLa cells were treated with 7 mg/mL *T. formosanum* for 16 h alone or in the presence of pretreated with indicated amounts of caffeine for 2 h, after which their cell lysates were subjected to (**A** and **B**) the list of up- and downregulated of (**A**) ribosomal protein genes (**B**) and RT-PCR analysis using primer pairs against the selected mRNAs, with *β-actin* mRNA as the mRNA loading and internal control. The green single-arrow is one of the target ribosomal proteins for further verification.

Our Figs. 2 and 5 suggested that it is an important issue of the treatment concentration and time of *T. formosanum* to address its effects on rRNAs, mRNAs, and proteins levels in HeLa cells. We failed to observe the rescue effect of caffeine on *T. formosanum*-suppressed mRNA expressions, even we could observe the rescue effect of caffeine on specific proteins (Fig. 5). It was also a puzzle for higher amounts of *T. formosanum* suppressed *GAPDH* and *β-actin* mRNAs, not both proteins. Hence, we sought to appropriate conditions of *T. formosanum* for the monitoring changes of all interesting mRNAs and proteins. In Fig. 7A, the value of RIN was 6.3 compared with 4.8 in the same treatment condition of 7 mg/mL *T. formosanum*-treated HeLa cells for 16 h (compared Fig. 1C with Fig. 5A). *Wild-type SRSF3* (*serine/arginine rich splicing factor 3*) (*SRSF3 WT*) mRNA is changed to exon 4-included premature *SRSF3* (*SRSF3 PTC*) mRNA by caffeine. SRSF3 is an important splicing factor for the expression of p53 protein α form and hypoxia inducible factor 1 alpha (HIF-1α)[40]. In Fig. 7B and C, *T. formosanum* suppressed *SRSF3*, *p53*, and *cyclin B1* mRNAs and proteins and induced *CHOP*

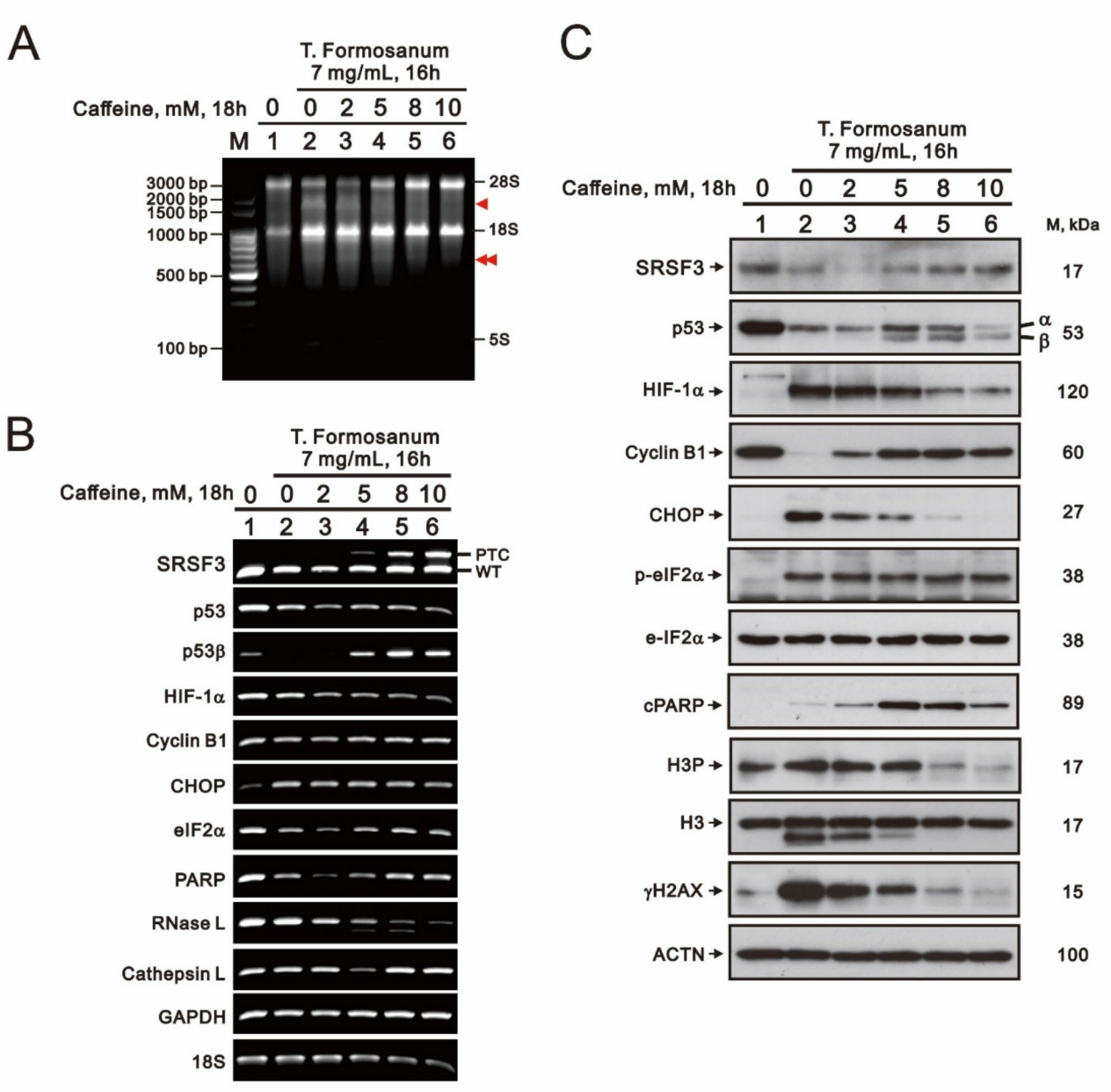

Fig. 7. The rescue effects of caffeine on the *T. formosanum*-dependent mRNAs and proteins in HeLa cells. (**A-C**) HeLa cells were treated with 7 mg/mL *T. formosanum* for 16 h alone or in the presence of pretreated with indicated amounts of caffeine for 2 h, after which their cell lysates were subjected to (**A**) total RNA agarose gel electrophoresis analysis; (**B**) RT-PCR analysis using primer pairs against the indicated mRNAs, with 18S rRNA as an internal control; (**C**) western blot analysis using antibodies against the indicated proteins, with ACTN as the protein loading control. The red single-arrow is the cleaved 28S rRNA and the double-arrow is the cleaved 18S rRNA. M, bp: the molecular weight of rRNA. M, kDa: the molecular weight of protein.

mRNA and protein. However, *T. formosanum* suppressed *HIF-1α*, *eIF2α*, and *poly(ADP-ribose) polymerase* (*PARP*) mRNAs, but increased HIF-1α, p-eIF2α, and cleaved PARP (cPARP) proteins. *T. formosanum* induced H3 clipping and γH2AX. proteins. Increasing amounts of caffeine differentially rescued or reversed the effect of p53β, HIF-1α, cyclin B1, CHOP, p-eIF2α, cPARP, H3 clipping, and γH2AX. proteins by *T. formosanum*. The rescue of *T. formosanum*-induced H3 clipping fragment by caffeine, accompanying with the decrease of H3P (phosphorylation of serine 10). Caffeine suppressed rRNA cleavage enzyme *RNase L* mRNA and H3 clipping enzyme *Cathepsin L*. Our data revealed that HIF-1α was a repressor for *cyclin B1* and activator for *CHOP* in HeLa cells, consistent with literatures. Caffeine regulated *cyclin B1* and *CHOP* mRNAs and proteins via the function role of HIF-1α.

To test whether *Taraxacum* induces histone H3 clipping in different cells. We treated human HeLa cervical cancer, human liver cancers, including Huh6, Huh7, HepG2, and Hep3B, human L0-2 normal liver cell line with different resources of *Taraxacum*. We identified the clipping fragment of histone H3 with two antibodies against H3 and H3P(S10) using the western blotting analysis (Fig. 8). Our data showed that H3 clipping fragments were found in HeLa, Huh6, and HepG2 cells treated with *T. formosanum* (fresh extract). The clipping status determined the sensitivity to H3P antibody.

The effects of caffeine on necrosis, apoptosis, autophagy, and mitochondrial depolarization by *T. formosanum* in human cervical HeLa cells

Our previous data showed that *T. formosanum* induced cell death, including necrosis and apoptosis[27]. Caffeine enhanced the cleaved PARP fragments by *T. formosanum* (Fig. 7C). We further analyzed the effect of *T. formosanum* on necrosis and apoptosis using 7-AAD/Annexin V flow-cytometry analysis (Fig. 9). Our data demonstrated that *T. formosanum* induced 88% necrotic and 13% late apoptotic populations and increasing amounts of caffeine significantly suppressed necrotic populations to 82%, $p(\text{ANOVA}) = 1.9 \times 10^{-5}$, and significantly enhanced late apoptotic populations 18%, $p(\text{ANOVA}) = 7.5 \times 10^{-6}$. *T. formosanum* and caffeine both had no effect on early apoptotic population (Fig. 9A). Caffeine had no apparent effect on the sum of necrotic and apoptotic populations by *T. formosanum* in HeLa cells. However, increasing amounts of caffeine had enhanced effects on the populations of Annexin V. This finding could be verified with the PE-Annexin V M1 gating data (Fig. 9B and C).

In addition to necrosis, apoptosis, and ER stress, we further analyzed the effects of *T. formosanum* on autophagy and mitochondrial membrane potential and examined whether caffeine had the ability to reverse its effects. We first analyzed the effect of *T. formosanum* on autophagy using the acridine orange dye with the flow-cytometry. We observed *T. formosanum* suppressed the endogenous autophagy (the formation of autophagolysosome), but caffeine reversed the suppression to relative endogenous level with the increasing amounts in HeLa cells (Fig. 10A and B). Then, we examined the effect of *T. formosanum* on mitochondrial membrane potential using the JC-1 dye with the flow-cytometry. Our data showed that *T. formosanum* disrupted mitochondrial membrane potential by the decreased red JC-1 aggregates and increased green JC-1 monomers (Fig. 10C). The red/green ratio apparently was decreased *T. formosanum* and rescued by caffeine in a dose-dependent manner. Lipidated LC3 (LC3B II) plays a crucial role in the closure of autophagosomes and facilitates the docking of specific cargos and adaptor proteins, such as p62. Our Fig. 10D western blotting data showed that the changes in p62 levels rather than with LC3BII/I in the presence of *T. formosanum* or in combination with caffeine correlated with the autophagy percentage we determined (reflecting autophagolysosome presence through acridine orange, Fig. 10B).

Discussion

The integrity of RNA molecules is crucial for experiments that aim to reflect the snapshot of gene expression at the moment of RNA extraction. The advent of microcapillary electrophoretic RNA separation now provides the basis for an automated high-throughput approach to estimate the RIN value in an unambiguous manner using an Agilent 2100 bioanalyzer[34]. In this study, we used both the ratio of 2 S/18S and RIN to confirm RNA molecule integrity. Our data showed that the quality of mRNA was the most easily degraded material compared to rRNA and protein. With the help of the RIN values, we could elucidate the effect of *T. formosanum* on the cleavage of rRNAs which was related to RSR. In addition to the activation of p38 and JNK signaling pathways, we identified the hallmark major spliceosome, ribosomal proteins, TNF-α signaling via NF-κB, inflammatory response, and IL6-JAK-STAT3 signaling with the analysis of RNA sequencing. Caffeine was the only screening drug to rescue the effect of *T. formosanum* on RSR mediated through the blockade of rRNA cleavage, the reduction of HIF-1α, CHOP, H3 clipping, and γH2AX proteins, and downregulation of *RNase L* and *cathepsin L* mRNAs. The rescue effects of caffeine were not mediated through cell death, but partly through autophagy, ER stress, and mitochondrial membrane potential.

In this study, we showed data that the quality of rRNA, such as cleaved 28S–18S rRNA fragments, affects the stability of mRNAs or/and protein synthesis, was disrupted by *Taraxacum*mediated through RSR. The cleaved rRNA fragments might serve as non-coding RNAs or long non-coding RNAs, as well as N-truncated histone H3, involved into the epigenetic regulation in cells[8,14,39,41]. Many studies demonstrated the importance of histone H3 clipping in various biological processes, such as ESCs and PBMCs, regulation of monocyte-to-macrophage differentiation, a novel signature of human neutrophil extracellular traps, and regulation of myoblast differentiation[15–19]. One of the most conserved mechanisms by which cells sense viral infection mediated through dsRNA related RSR to trigger antiviral and inflammatory immune responses[3–6]. Our data showed that caffeine had the ability to rescue the effects of *T. formosanum* on the rRNA cleavage and histone H3 N-tail clipping events. Our findings suggest that it is important to identify whether the working mechanisms of rRNA cleavage and histone H3 N-tail clipping are mediated through similar or common enzymes. Hence, the differentiation of human THP-1 cells from monocyte to macrophage by phorbol 12-myristate acetate or

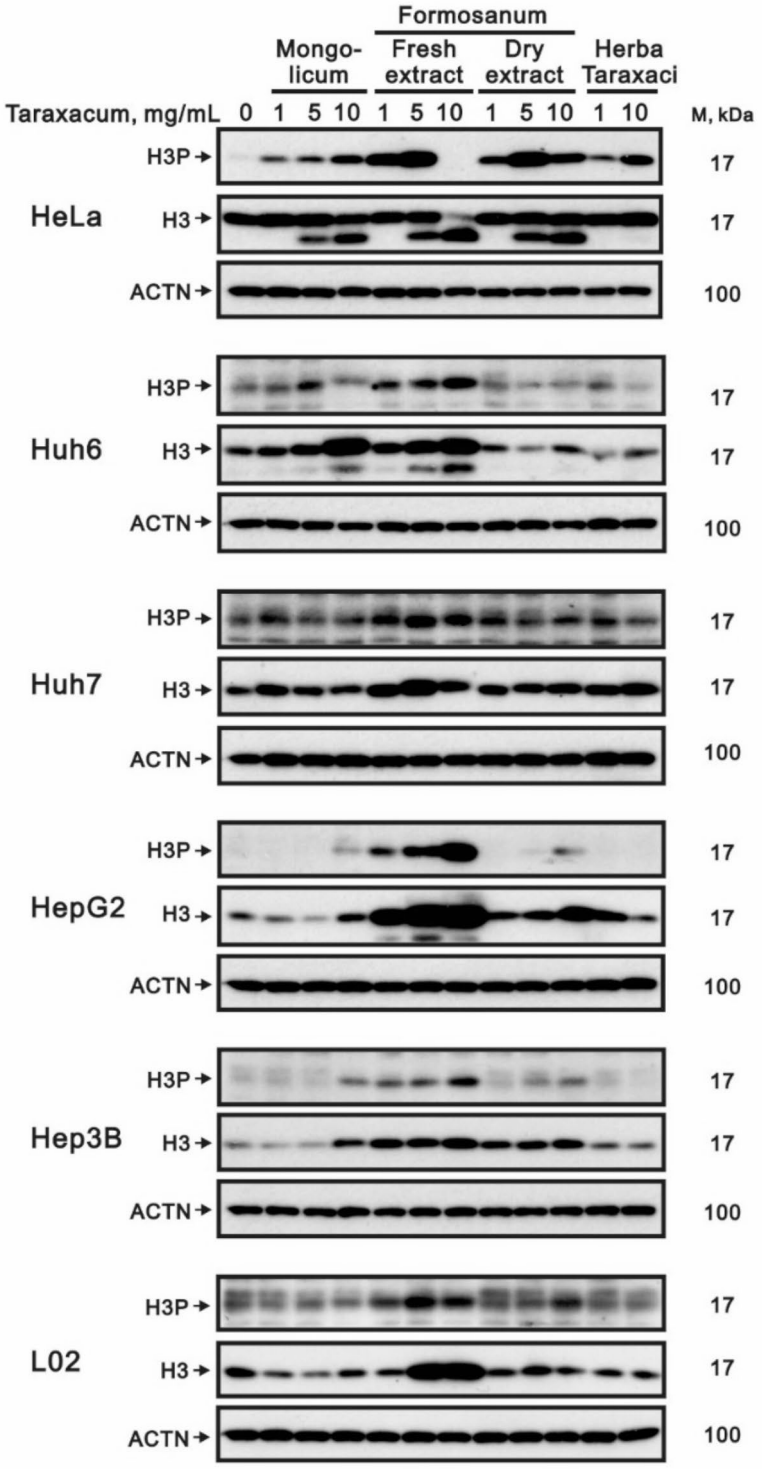

Fig. 8. Effects of *Taraxacum* on histone H3 status in various cells. HeLa, Huh6, Huh7, HepG2, Hep3B, and L02 cells were treated for 24 h with the indicated concentrations of *T. mongolicum*, *T. formosanum*, or *Herba Taraxaci*. These cell lysates were subjected to western blot analysis using antibodies against the indicated proteins, with ACTN as the protein loading control. M, kDa: the molecular weight of protein.

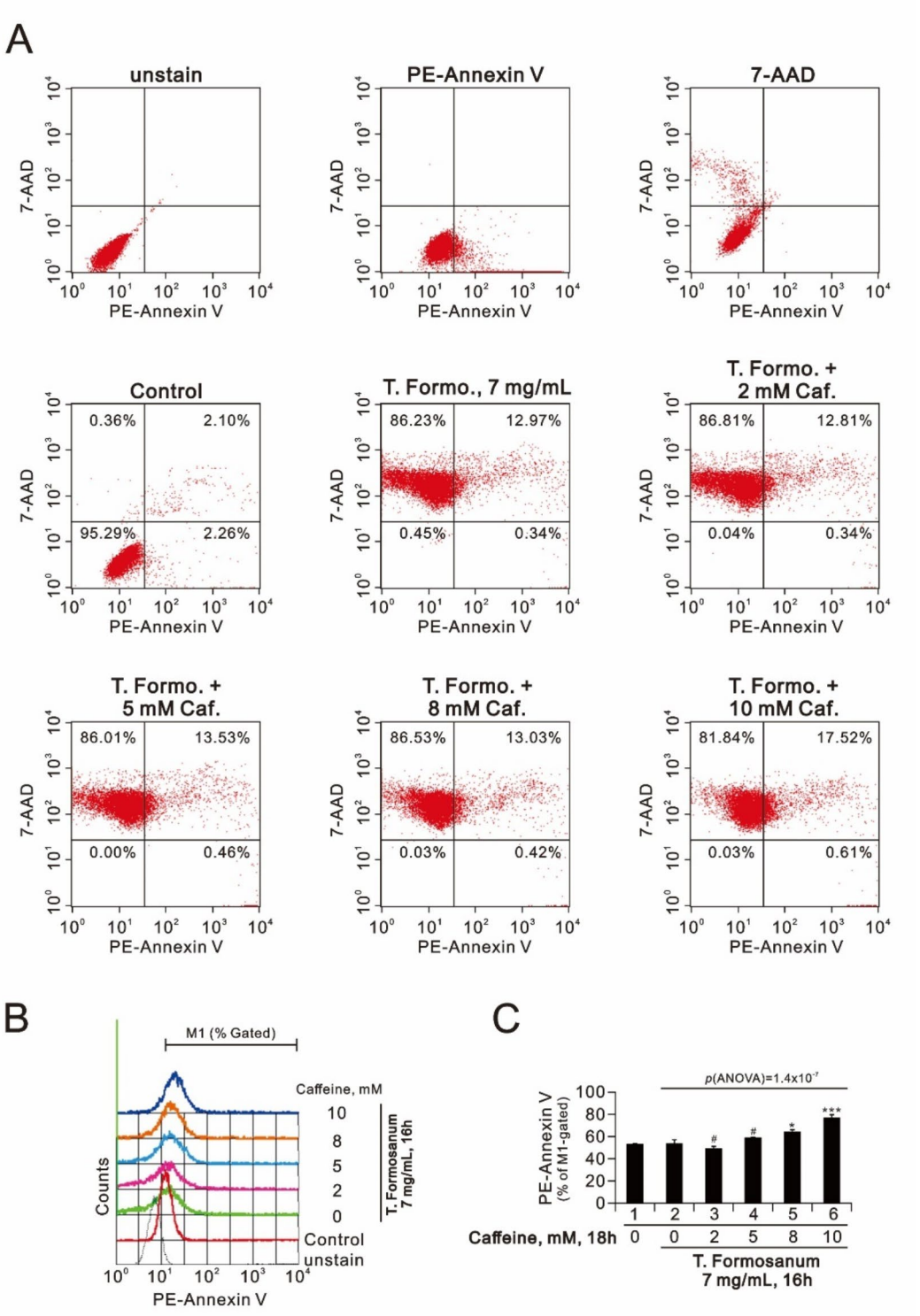

Fig. 9. The effects of caffeine on the *T. formosanum*-dependent necrosis and apoptosis in HeLa cells. HeLa cells were treated with 7 mg/mL *T. formosanum* for 16 h alone or in the presence of pretreated with indicated amounts of caffeine for 2 h. Collected cells were subject to the flow-cytometry analysis for (**A**) necrosis and apoptosis analysis with 7-AAD/Annexin V kit. (**B** and **C**) Cells stained with PE-Annexin V were gated and plotted. The results are representative of three independent experiments. #$p > 0.05$, *$p < 0.05$, and ***$p < 0.001$ (Student's t-test).

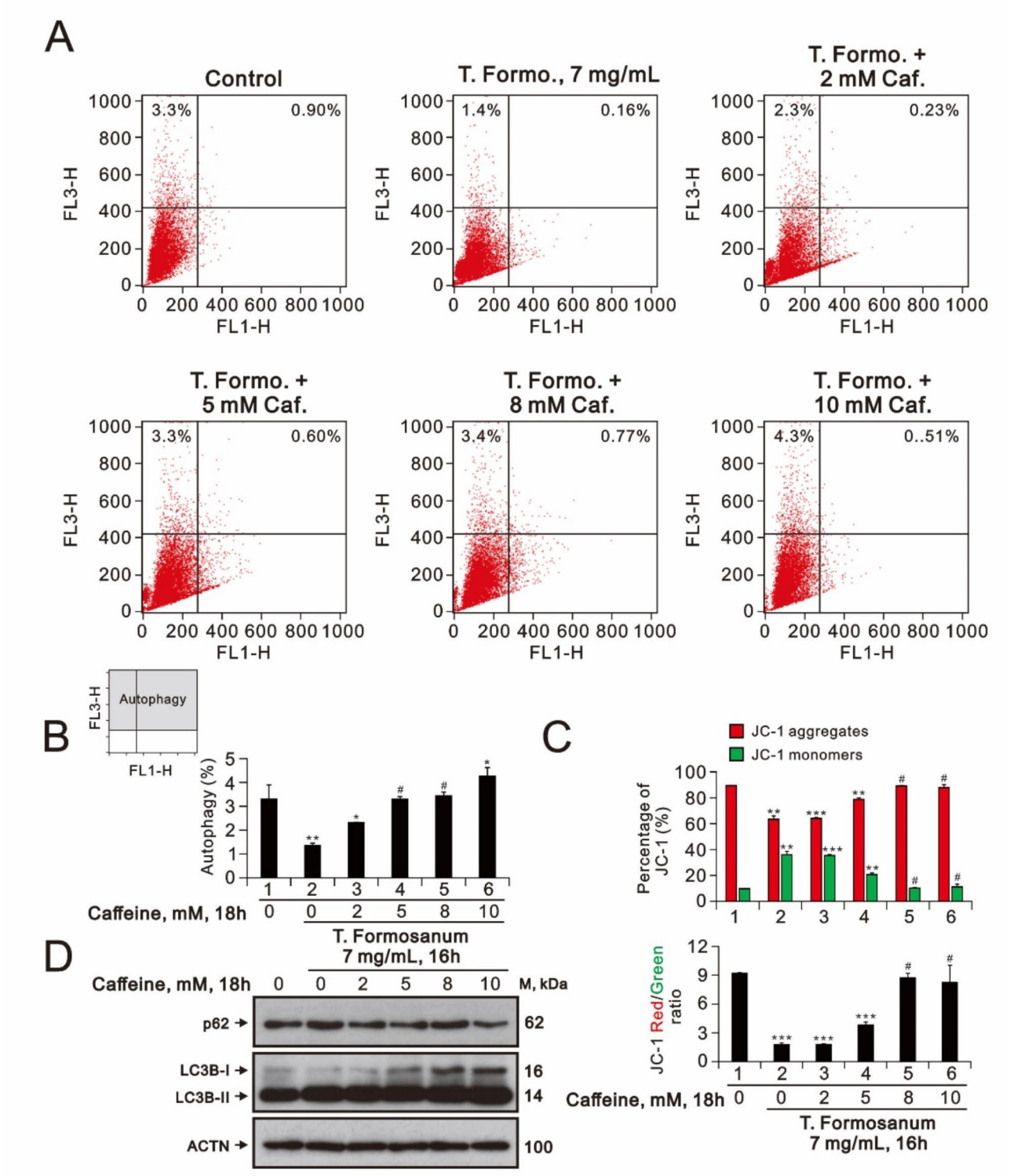

Fig. 10. The effects of caffeine on the *T. formosanum*-dependent autophagy and mitochondrial membrane potential in HeLa cells. HeLa cells were treated with 7 mg/mL *T. formosanum* for 16 h alone or in the presence of pretreated with indicated amounts of caffeine for 2 h. Collected cells were subject to the flowcytometry analysis for (**A** and **B**) autophagy and (**C**) mitochondrial membrane potential with AO and JC-1 dyes, respectively. The results are representative of three independent experiments. #$p > 0.05$, *$p < 0.05$, **$p < 0.01$, and ***$p < 0.001$ (Student's t-test). (**D**) These cell lysates were subjected to western blot analysis using antibodies against the indicated proteins, with ACTN as the protein loading control. M, kDa: the molecular weight of protein.

rat C2C12 myoblast cells by 2% horse serum should be a good platform to examine the event timing of rRNA cleavage and histone H3 N-tail clipping in cells.

The RSR is activated by ribosomal impairment, which can disrupt protein synthesis, increase inflammatory signaling, and even lead to cell death if left unresolved[2,42]. RNase L of 2-5AMD cleaves a broad spectrum of host RNAs and the cleavage of rRNA does not inhibit the activity of the ribosome, whereas it might reduce ~90% mRNA levels in the cell[10]. In addition, mRNA decay fragments via the NMD are to produce short peptides or functional truncated proteins[43]. In current study, we failed to provide direct evidence of RNase L involved in the cleavage of 28S rRNA or Cathepsin L involved in the clipping of histone H3 induced by *T. formosanum* and the rescue by caffeine. Compared with the well-known cleaved at amino acid residue A21 of histone H3, our western botting data showed that the N-truncated fragment was detected with dimethyl H3(K79) antibody, not H3P antibody. Therefore, the RIN value, the status of histone H3, and the alternative splicing of SRSF3 provide the hint on the quality of total RNA, the epigenetic status of H3, and the SRSF3 isoform for the expression levels of various mRNAs and proteins. It should be a challenge to identify non-coding RNAs from the cleavage site(s) of rRNAs and histone H3 and enzymes for the cleavage of rRNAs and the clipping of histone H3.

Our current data support the notion that *T. formosanum* induces apoptotic and necrotic cell death by disrupting the mitochondrial membrane potential and inhibiting autophagy formation. However, caffeine, a rescue agent, can reverse the effects of *T. formosanum* on mitochondrial membrane potential and autophagy. Nevertheless, caffeine fails to decrease cell death, resulting in an increasing percentage of late apoptosis and a decreasing percentage of necrosis. It would be interesting to investigate the order of autophagy, mitochondrial dysfunction, or apoptosis in the presence of *T. formosanum*, caffeine, or both combinations. It will elucidate the mechanisms of gene regulation from cleaved rRNAs and N-truncated histone H3 to mRNAs, and their respective cellular death and survival stresses.

Cellular stresses can lead to damage of RNAs by modifying, mutating, or cleaving them, resulting in the production of non-functional proteins that can be harmful to cells[44]. Ribosome collisions caused by various RNA damages are a key regulator of specific stress response pathways. For example, low doses of the translational elongation inhibitor anisomycin increase the frequency of ribosome collisions, triggering cellular recovery through integrated stress response. On the other hand, high doses of anisomycin lead to persistent ribosome stalling, causing apoptosis through the activation of MAPK signaling cascades due to 28S rRNA damage[1,42]. Three mRNA surveillance pathways, NMD, no-go decay, and non-stop decay, play crucial roles in resolving translation problems that can arise from faulty mRNAs or defective ribosomes[41,45,46]. Our current data indicate that *T. formosanum* induces a RSR, resulting in 28S rRNA cleavage to degrade most of mRNAs but which still partly express their proteins. *T. formosanum* also modulates ribosomal proteins and splicing pathways. Hence, investigating the involvement of non-coding RNA, ribosome collision, and mRNA surveillance pathways by *T. formosanum* in cells is a task for future research.

In summary, we first used the RIN value and 28S/18S ratio to confirm the *Taraxacum*-induced rRNA cleavage. In addition to the activation of p38 and JNK signaling pathways, we identified the hallmark major spliceosome, ribosomal proteins, TNF-α signaling via NF-κB, inflammatory response, and IL6-JAK-STAT3 signaling with the analysis of RNA sequencing. Caffeine was the only screening drug to rescue the effect of *T. formosanum* on RSR mediated through the blockade of rRNA cleavage, the reduction of HIF-1α, CHOP, H3 clipping, and γH2AX proteins, and downregulation of *RNase L* and *cathepsin L* mRNAs. The rescue effects of caffeine were not mediated through cell death, but partly through autophagy, ER stress, and mitochondrial membrane potential. By providing detailed information on *Taraxacum*-induced rRNA cleavage and N-truncated histone H3's mechanisms of gene regulation, we hope to understand their respective cellular death and survival stresses.

Materials and methods

Preparation of aqueous extracts of Taraxacum

The dried whole *T. mongolicum* plants were purchased from the Yu Hong Biotechnology Company (Chiayi, Taiwan, ROC). *T. formosanum* is distributed mainly in the coastal areas of north Taichung in Taiwan. The whole *T. formosanum* plants were collected and identified by Dr. Rong-Chi Yang, Adjunct Associate Professor, School of Traditional Chinese Medicine, Chang Gung University (Taoyuan, Taiwan, ROC). *T. mongolicum* and *T. formosanum* of this study complied with the National Defense Medical Center's, Taiwan's, and international guidelines, including the IUCN Policy Statement on Research Involving Species at Risk of Extinction and the Convention on the Trade in Endangered Species of Wild Fauna and Flora. One hundred grams of the dried whole *T. mongolicum* and *T. formosanum*plants were crushed and prepared as previously described[27]. All *Taraxacum* powders were dissolved in boiled ddH_2O to the desired final concentration (mg/ml) for cell treatment previously outlined[27].

Cell culture and chemicals

HeLa, HepG2, Hep3B, Huh6, Huh7, and L02 cells were obtained from the American Type Culture Collection (ATCC; Manassas, VA, USA) and cultured in Dulbecco's modified Eagle's medium (DMEM) supplemented with 10% fetal bovine serum (FBS) and 1% penicillin-streptomycin (Invitrogen, USA). Actinomycin D, acridine orange, AG1478, ALLM, ammonium chloride, BI-D1870, caffeine, ellagic acid, LY294002, MG132, ouabain, PD98059, PFT-α, resveratrol, SB203580, and Z-VAD-FMK were purchased from Sigma Aldrich (MO, USA).

Western blot analysis

Cells were lysed in Radio-Immunoprecipitation Assay buffer (100 mM Tris-HCl pH 8.0, 150 mM NaCl, 0.1% SDS, and 1% Triton 100) at 4 °C. Protein concentrations were measured using a DC Protein Assay Kit (Bio-Rad Laboratories, USA). Proteins in aliquots of the lysate were separated by SDS-PAGE and electro-transferred

to PVDF membranes (Immobilon-P; Millipore, Bedford, MA, USA) using a Bio-Rad Semi-Dry Transfer Cell. The blots were then incubated with primary antibodies against α-actinin (ACTN), p53, cyclin B1, p62 (Santa Cruz Biotechnology, USA); HIF-1α, CHOP, eIF2α, peIF2α, PARP, H3, H3P, Di-methyl-H3 (K79), LC3B (Cell Signaling, USA); γH2AX, cyclin D1, and p21 (Abcam, Cambridge, UK); SRSF3 (WH0006428M8, Sigma-Aldrich). Thereafter, the blots were incubated with HRP-conjugated secondary antibodies (anti-mouse IgG, AP192P; and anti-rabbit IgG, AP132P, Merck-Millipore). The immunoreactive proteins were detected using ECL™ Western Blotting Detection Reagents and Amersham Hyperfilm™ ECL (GE Healthcare, USA) as previously described[47].

Reverse transcription-polymerase chain reaction (RT-PCR)

Total RNAs were isolated from HeLa cells using TRIzol reagent (Invitrogen). Reverse transcription for first strand cDNA synthesis was carried out using MMLV reverse transcriptase (Epicentre Biotechnologies, USA) with 1 μg of total RNA for 60 min at 37 °C. The PCR reactions were run on a Veriti Thermal Cycler (Applied Biosystems, USA), as previously described[47]. The PCR primers are listed below.

Primer name	Sequence (5'◊3')
p53	Forward: 5'-CTCTGACTGTACCACCATCCACTA-3' Reverse: 5'-GAGTTCCAAGGCCTCATTCAGCTC-3'
cyclin D1	Forward: 5'-ATGGAACACCAGCTCCTGTGCTGC-3' Reverse: 5'-TCAGATGTCCACGTCCCGCACGTCGG-3'
p21	Forward: 5'-CTGAGCCGCGACTGTGATGCG-3' Reverse: 5'-GGTCTGCCGCCGTTTTCGACC-3'
CHOP	Forward: 5'-CATTGCCTTTCTCCTTCGGG-3' Reverse: 5'-GCCGTTCATTCTCTTCAGCT-3'
GAPDH	Forward: 5'-CTTCATTGACCTCAACTAC-3' Reverse: 5'-GCCATCCACAGTCTTCTG-3'
18S	Forward: 5'-CAGCCACCCGAGATTGAGCA-3' Reverse: 5'-TAGTAGCGACGGGCGGTGTG-3'
β-actin	Forward: 5'-GTGGGGCGCCCCAGGCACCA-3' Reverse: 5'-CTCCTTAATGTCACGCACGATTTC-3'
Cyclin B1	Forward: 5'-GTTGATACTGCCTCTCCAAG-3' Reverse: 5'-CTTAGTATAAGTGTTGTCAGTCAC-3'
HIF-1α	Forward: 5'-GAACCTGATGCTTTAACT-3' Reverse: 5'-CAACTGATCGAAGGAACG-3'
IL-6	Forward: 5'-ATGAACTCCTTCTCCACAAGCGC-3 Reverse: 5'-CTACATTTGCCGAAGAGCCCTCA-3'
H3	Forward: 5'-ATGGCTCGCACTAAGCAAACTG-3' Reverse: 5'-TCACGCCCTCTCTCCGCGGA-3'
RPL3	Forward: 5'-GTACTGCCAAGTCATCCGTG-3' Reverse: 5'-CGGTGATGGTAGCCTTTCTG-3'
RPL4	Forward: 5'-GATACGCCATCTGTTCTGCC-3' Reverse: 5'-CGCCAAGTGCCGTACAATTC-3'
RPL6	Forward: 5'-GCAAGAGGGTGGTTTTCCTG-3' Reverse: 5'-GAGCAAACACAGATCGCAGG-3'
RPS2	Forward: 5'-GAGGCTACTGGGGGAACAAG-3' Reverse: 5'-GTGTGGGTCTTGACGAGGTG-3'
RPS26	Forward: 5'-GAAGGAACAATGGTCGTGCC-3' Reverse: 5'-TTACATGGGCTTTGGTGGGG-3'
SRSF3	Forward: 5'-ATGCATCGTGATTCCTGTCCATTG-3' Reverse: 5'-CTATTTCCTTTCATTTGACCTAGATC-3'
p53β	Forward: 5'-ATGGAGGAGCCGCAGTCAGAT-3' Reverse: 5'-TTTGAAAGCTGGTCTGGTCCTGA-3'
eIF2α	Forward: 5'-ACCTCAGAATGCCGGGTCTA-3' Reverse: 5'-GTGGGGTCAAGCGCCTATTA-3'
PARP	Forward: 5'-CAGAAGTACGTGCAAGGGGT-3' Reverse: 5'-GGCACTTGCTGCTTGTTGAAG-3'
RNase L	Forward: 5'-TGGACGGCTGGTCCTCTATG-3' Reverse: 5'-CTGTGGGTTTGGGGGAAATGC-3'
Cathepsin L	Forward: 5'-GATGGAGGAGAGCAGTGTGG-3' Reverse: 5'-GCAGCCTTCATTGCCTTGAG-3'

Fluorescence-activated cell sorting (FACS), apoptosis, autophagy, and mitochondrial membrane potential analysis

Early and late stages of apoptotic cells were evaluated by a fluorescein Phycoerythrin (PE)-Annexin V Apoptosis Detection Kit (BD Biosciences) according to the manufacturer's protocol. Cells are stained with PE-Annexin V as well as 7-Amino-Actinomycin (7-AAD) to determine the effects of indicated drugs (*T. formosanum* and caffeine) on early apoptosis (PE-Annexin positive and 7-AAD negative), late apoptosis (PE-Annexin positive and 7-AAD positive), and necrosis (PE-Annexin negative and 7-AAD positive), as previously described[47].

The acidic compartments of the cells were detected using acridine orange (Sigma, Cat. No. A8097) staining and measured by flow cytometry. As the protonated form of acridine orange accumulates inside acidic vesicles, it is a marker for the final steps of the autophagy process. Briefly, the cells were treated with the indicated lidocaine dosages for 24 h, stained with acridine orange (1 μg/mL) for 20 min at 37 °C, and then trypsinized for harvesting. Afterwards, the cells were washed once with PBS, resuspended in 400 μl of PBS, and then analyzed via flow cytometry (FACSCalibur, BD, Biosciences). The excitation wavelength was 488 nm and fluorescence were detected at 510–530 nm (green fluorescence, FL1) and 650 nm (red fluorescence, FL3). The data were analyzed using the CellQuest™ software program. The percentage of autophagy cells was calculated based on the number of cells present in the upper-left and upper-right quadrants, as previously described[48].

Mitochondrial membrane potential was monitored using the MitoScreen (JC-1) kit (BD Pharmingen). After being treated with drugs, dead and live cells were collected, and JC-1 solution was added prior to the 15 min incubation. The cells were then washed twice with a binding buffer. Each sample was evaluated using the FACSCalibur flow cytometer and Cell Quest Pro software, as previously described[49].

RNA sequencing and analysis

Total RNA of each sample was extracted using TRIzol Reagent and RNeasy Mini Kit (Qiagen). Total RNA of each sample was quantified and qualified by Agilent 2100/2200 Bioanalyzer (Agilent Technologies, Palo Alto, CA, USA) and NanoDrop (Thermo Fisher Scientific Inc.). 1 μg total RNA with a RIN value above 6.5 was used for following library preparation[34]. Next generation sequencing library preparations were constructed according to the manufacturer's protocol and previously described[50]. The poly(A) mRNA isolation was performed using Poly(A) mRNA Magnetic Isolation Module or rRNA removal Kit. The mRNA fragmentation and priming were performed using First Strand Synthesis Reaction Buffer and Random Primers. First strand cDNA was synthesized using ProtoScript II Reverse Transcriptase and the second-strand cDNA was synthesized using Second Strand Synthesis Enzyme Mix. The purified double-stranded cDNA by beads was then treated with End Prep Enzyme Mix to repair both ends and add a dA-tailing in one reaction, followed by a T-A ligation to add adaptors to both ends. Size selection of Adaptor-ligated DNA was then performed using beads, and fragments of ~400 bp (with the approximate insert size of 300 bp) were recovered. Each sample was then amplified by PCR using P5 and P7 primers, with both primers carrying sequences which can anneal with flow cell to perform bridge PCR and P5/P7 primer carrying index allowing for multiplexing. The PCR products were cleaned up using beads, validated using an Qsep100 (Bioptic, Taiwan), and quantified by Qubit 3.0 Fluorometer (Invitrogen, Carlsbad, CA, USA). Then libraries with different indices were multiplexed and loaded on an Illumina HiSeq/Novaseq instrument according to manufacturer's instructions (Illumina, San Diego, CA, USA). Sequencing was carried out using a 2 × 150 paired-end configuration; image analysis and base calling were conducted by the HiSeq Control Software + OLB + GAPipeline-1.6 (Illumina) on the HiSeq instrument. The sequences were processed and analyzed by GENEWIZ.

Differential Gene expression analysis and Gene Set Enrichment Analysis (GSEA)

Differential expression analysis used the DESeq2 Bioconductor package, a model based on the negative binomial distribution. the estimates of dispersion and logarithmic fold changes incorporate data-driven prior distributions, Padj of genes were set < 0.05 to detect differential expressed ones. To comprehensively evaluate gene expression changes related to *T. formosanum*and caffeine in HeLa cells, we performed ranked gene list analyses using GSEA software version 4.3.2. Genes were ranked based on the t-statistic and analyzed through pre-ranked analysis using the gene set enrichment analysis software, along with the Hallmark gene set from MSigDB v2023.1.Hs. For detailed software settings, please refer to the previous article[5152].

Statistical analysis

The values are expressed as the mean ± SD of at least three independent experiments. All the comparisons between groups were conducted using the Student's t-tests and comparison among multiple groups was conducted using analysis of variance (ANOVA) with SPSS 20.0 for Windows (SPSS, Chicago, IL). The statistical significance was set at $p < 0.05$.

Data availability

The datasets generated during and/or analyzed during the current study are available from the corresponding author on reasonable request. Our RNA-seq data were also deposited into the NCBI Gene Expression Omnibus (accession number GSE263110).

Received: 29 July 2024; Accepted: 6 January 2025
Published online: 21 January 2025

References

1. Iordanov, M. S. et al. Ribotoxic stress response: activation of the stress-activated protein kinase JNK1 by inhibitors of the peptidyl transferase reaction and by sequence-specific RNA damage to the alpha-sarcin/ricin loop in the 28S rRNA. *Mol. Cell. Biol.* **17**, 3373–3381. https://doi.org/10.1128/MCB.17.6.3373 (1997).
2. Vind, A. C., Genzor, A. V. & Bekker-Jensen, S. Ribosomal stress-surveillance: three pathways is a magic number. *Nucleic Acids Res.* **48**, 10648–10661. https://doi.org/10.1093/nar/gkaa757 (2020).
3. Smith, W. E. et al. Shiga toxin 1 triggers a ribotoxic stress response leading to p38 and JNK activation and induction of apoptosis in intestinal epithelial cells. *Infect. Immun.* **71**, 1497–1504. https://doi.org/10.1128/IAI.71.3.1497-1504.2003 (2003).
4. Korcheva, V., Wong, J., Corless, C., Iordanov, M. & Magun, B. Administration of ricin induces a severe inflammatory response via nonredundant stimulation of ERK, JNK, and P38 MAPK and provides a mouse model of hemolytic uremic syndrome. *Am. J. Pathol.* **166**, 323–339. https://doi.org/10.1016/S0002-9440(10)62256-0 (2005).

5. Elsea, C. R., Roberts, D. A., Druker, B. J. & Wood, L. J. Inhibition of p38 MAPK suppresses inflammatory cytokine induction by etoposide, 5-fluorouracil, and doxorubicin without affecting tumoricidal activity. *PLoS One*. **3**, e2355. https://doi.org/10.1371/journal.pone.0002355 (2008).
6. Iordanov, M. S. et al. Ultraviolet radiation triggers the ribotoxic stress response in mammalian cells. *J. Biol. Chem.* **273**, 15794–15803. https://doi.org/10.1074/jbc.273.25.15794 (1998).
7. Gagliardi, D. & Dziembowski, A. 5' and 3' modifications controlling RNA degradation: from safeguards to executioners. *Philos. Trans. R Soc. Lond. B Biol. Sci.* **373**, 20180160. https://doi.org/10.1098/rstb.2018.0160 (2018).
8. Seal, R. L. et al. A guide to naming human non-coding RNA genes. *EMBO J.* **39**, e103777. https://doi.org/10.15252/embj.2019103777 (2020).
9. Houge, G. et al. Fine mapping of 28S rRNA sites specifically cleaved in cells undergoing apoptosis. *Mol. Cell. Biol.* **15**, 2051–2062. https://doi.org/10.1128/MCB.15.4.2051 (1995).
10. Rath, S. et al. Concerted 2-5A-Mediated mRNA decay and transcription reprogram protein synthesis in the dsRNA response. *Mol. Cell.* **75**, 1218–1228. https://doi.org/10.1016/j.molcel.2019.07.027 (2019). e1216.
11. Burke, J. M., Moon, S. L., Matheny, T., Parker, R. & RNase L Reprograms Translation by Widespread mRNA Turnover Escaped by Antiviral mRNAs. *Mol Cell* 75, 1203–1217 e1205 (2019). https://doi.org/10.1016/j.molcel.2019.07.029
12. Tan, K., Stupack, D. G. & Wilkinson, M. F. Nonsense-mediated RNA decay: an emerging modulator of malignancy. *Nat. Rev. Cancer*. **22**, 437–451. https://doi.org/10.1038/s41568-022-00481-2 (2022).
13. Karasik, A., Jones, G. D., DePass, A. V. & Guydosh, N. R. Activation of the antiviral factor RNase L triggers translation of non-coding mRNA sequences. *Nucleic Acids Res.* **49**, 6007–6026. https://doi.org/10.1093/nar/gkab036 (2021).
14. Millan-Zambrano, G., Burton, A., Bannister, A. J. & Schneider, R. Histone post-translational modifications - cause and consequence of genome function. *Nat. Rev. Genet.* **23**, 563–580. https://doi.org/10.1038/s41576-022-00468-7 (2022).
15. Shen, J. et al. JMJD5 cleaves monomethylated histone H3 N-tail under DNA damaging stress. *EMBO Rep.* **18**, 2131–2143. https://doi.org/10.15252/embr.201743892 (2017).
16. Howe, C. G. & Gamble, M. V. Enzymatic cleavage of histone H3: a new consideration when measuring histone modifications in human samples. *Clin. Epigenetics*. **7**, 7. https://doi.org/10.1186/s13148-014-0041-5 (2015).
17. Vossaert, L. et al. Identification of histone H3 clipping activity in human embryonic stem cells. *Stem Cell. Res.* **13**, 123–134. https://doi.org/10.1016/j.scr.2014.05.002 (2014).
18. Santos-Rosa, H. et al. Histone H3 tail clipping regulates gene expression. *Nat. Struct. Mol. Biol.* **16**, 17–22. https://doi.org/10.1038/nsmb.1534 (2009).
19. Duncan, E. M. et al. Cathepsin L proteolytically processes histone H3 during mouse embryonic stem cell differentiation. *Cell* **135**, 284–294. https://doi.org/10.1016/j.cell.2008.09.055 (2008).
20. Rice, J. C. et al. MMP-2 is a novel histone H3 N-terminal protease necessary for myogenic gene activation. *Epigenetics Chromatin*. **14**, 23. https://doi.org/10.1186/s13072-021-00398-4 (2021).
21. Ferrari, K. J. et al. Intestinal differentiation involves cleavage of histone H3 N-terminal tails by multiple proteases. *Nucleic Acids Res.* **49**, 791–804. https://doi.org/10.1093/nar/gkaa1228 (2021).
22. Martinez, M. et al. Taraxacum officinale and related species-An ethnopharmacological review and its potential as a commercial medicinal plant. *J. Ethnopharmacol.* **169**, 244–262. https://doi.org/10.1016/j.jep.2015.03.067 (2015).
23. Sharifi-Rad, M. et al. Ethnobotany of the genus Taraxacum-Phytochemicals and antimicrobial activity. *Phytother Res.* **32**, 2131–2145. https://doi.org/10.1002/ptr.6157 (2018).
24. Park, C. M., Park, J. Y., Noh, K. H., Shin, J. H. & Song, Y. S. Taraxacum officinale Weber extracts inhibit LPS-induced oxidative stress and nitric oxide production via the NF-kappaB modulation in RAW 264.7 cells. *J. Ethnopharmacol.* **133**, 834–842. https://doi.org/10.1016/j.jep.2010.11.015 (2011).
25. Xu, D. P. et al. Natural antioxidants in Foods and Medicinal plants: extraction, Assessment and resources. *Int. J. Mol. Sci.* **18**, 96. https://doi.org/10.3390/ijms18010096 (2017).
26. Gonzalez-Castejon, M., Visioli, F. & Rodriguez-Casado, A. Diverse biological activities of dandelion. *Nutr. Rev.* **70**, 534–547. https://doi.org/10.1111/j.1753-4887.2012.00509.x (2012).
27. Lin, C. J. et al. Anticancer effects of Taraxacum via cell cycle arrest, necrosis, apoptosis, and endoplasmic reticulum stress. *Am. J. Chin. Med.* **50**, 569–587. https://doi.org/10.1142/S0192415X22500227 (2022).
28. Lin, C. J. et al. Characteristics of the cytotoxicity of Taraxacum mongolicum and Taraxacum formosanum in human breast Cancer cells. *Int. J. Mol. Sci.* **23**, 11918. https://doi.org/10.3390/ijms231911918 (2022).
29. Bonora, M., Giorgi, C. & Pinton, P. Molecular mechanisms and consequences of mitochondrial permeability transition. *Nat. Rev. Mol. Cell. Biol.* **23**, 266–285. https://doi.org/10.1038/s41580-021-00433-y (2022).
30. Yu, L., Chen, Y. & Tooze, S. A. Autophagy pathway: Cellular and molecular mechanisms. *Autophagy* **14**, 207–215. https://doi.org/10.1080/15548627.2017.1378838 (2018).
31. Palikaras, K., Lionaki, E. & Tavernarakis, N. Mechanisms of mitophagy in cellular homeostasis, physiology and pathology. *Nat. Cell. Biol.* **20**, 1013–1022. https://doi.org/10.1038/s41556-018-0176-2 (2018).
32. Rambold, A. S. & Lippincott-Schwartz, J. Mechanisms of mitochondria and autophagy crosstalk. *Cell. Cycle*. **10**, 4032–4038. https://doi.org/10.4161/cc.10.23.18384 (2011).
33. Bloemberg, D. & Quadrilatero, J. Autophagy, apoptosis, and mitochondria: molecular integration and physiological relevance in skeletal muscle. *Am. J. Physiol. Cell. Physiol.* **317**, C111–C130. https://doi.org/10.1152/ajpcell.00261.2018 (2019).
34. Schroeder, A. et al. The RIN: an RNA integrity number for assigning integrity values to RNA measurements. *BMC Mol. Biol.* **7**, 3. https://doi.org/10.1186/1471-2199-7-3 (2006).
35. Zhang, J. et al. Hypoxia attenuates Hsp90 inhibitor 17-DMAG-induced cyclin B1 accumulation in hepatocellular carcinoma cells. *Cell. Stress Chaperones*. **21**, 339–348. https://doi.org/10.1007/s12192-015-0664-2 (2016).
36. Delbrel, E. et al. HIF-1alpha triggers ER stress and CHOP-mediated apoptosis in alveolar epithelial cells, a key event in pulmonary fibrosis. *Sci. Rep.* **8**, 17939. https://doi.org/10.1038/s41598-018-36063-2 (2018).
37. Kaida, D. et al. U1 snRNP protects pre-mRNAs from premature cleavage and polyadenylation. *Nature* **468**, 664–668. https://doi.org/10.1038/nature09479 (2010).
38. Mabin, J. W., Lewis, P. W., Brow, D. A. & Dvinge, H. Human spliceosomal snRNA sequence variants generate variant spliceosomes. *RNA* **27**, 1186–1203. https://doi.org/10.1261/rna.078768.121 (2021).
39. Chen, Y. G. & Hur, S. Cellular origins of dsRNA, their recognition and consequences. *Nat. Rev. Mol. Cell. Biol.* **23**, 286–301. https://doi.org/10.1038/s41580-021-00430-1 (2022).
40. Lu, G. Y. et al. Caffeine induces tumor cytotoxicity via the regulation of alternative splicing in subsets of cancer-associated genes. *Int. J. Biochem. Cell. Biol.* **47**, 83–92. https://doi.org/10.1016/j.biocel.2013.12.004 (2014).
41. De, S. & Muhlemann, O. A comprehensive coverage insurance for cells: revealing links between ribosome collisions, stress responses and mRNA surveillance. *RNA Biol.* **19**, 609–621. https://doi.org/10.1080/15476286.2022.2065116 (2022).
42. Wu, C. C., Peterson, A., Zinshteyn, B., Regot, S. & Green, R. Ribosome Collisions Trigger General Stress Responses to Regulate Cell Fate. *Cell* 182, 404–416 e414 (2020). https://doi.org/10.1016/j.cell.2020.06.006
43. Lykke-Andersen, S. & Jensen, T. H. Nonsense-mediated mRNA decay: an intricate machinery that shapes transcriptomes. *Nat. Rev. Mol. Cell. Biol.* **16**, 665–677. https://doi.org/10.1038/nrm4063 (2015).
44. Yan, L. L. & Zaher, H. S. How do cells cope with RNA damage and its consequences? *J. Biol. Chem.* **294**, 15158–15171. https://doi.org/10.1074/jbc.REV119.006513 (2019).

45. Morris, C., Cluet, D. & Ricci, E. P. Ribosome dynamics and mRNA turnover, a complex relationship under constant cellular scrutiny. *Wiley Interdiscip Rev. RNA*. **12**, e1658. https://doi.org/10.1002/wrna.1658 (2021).
46. Monaghan, L., Longman, D. & Caceres, J. F. Translation-coupled mRNA quality control mechanisms. *EMBO J.* **42**, e114378. https://doi.org/10.15252/embj.2023114378 (2023).
47. Wu, T. M. et al. Mechanisms and applications of the anti-cancer effect of pharmacological ascorbic acid in Cervical Cancer cells. *Front. Oncol.* **10**, 1483. https://doi.org/10.3389/fonc.2020.01483 (2020).
48. Hsu, Y. P. et al. Glucosamine and Silibinin Alter Cartilage Homeostasis through Glycosylation and Cellular stresses in human chondrocyte cells. *Int. J. Mol. Sci.* **25**, 4905. https://doi.org/10.3390/ijms25094905 (2024).
49. Fan, H. L. et al. In Vitro Cell Density determines the sensitivity of Hepatocarcinoma Cells to Ascorbate. *Front. Oncol.* **12**, 843742. https://doi.org/10.3389/fonc.2022.843742 (2022).
50. Fan, C. N. et al. Transcriptomic analysis reveals Cilostazol's role in ameliorating cardiovascular disease: inhibition of monocyte-to-macrophage differentiation and reduction of endothelial cell reactive oxygen species production. *Heliyon* **10**, e29194. https://doi.org/10.1016/j.heliyon.2024.e29194 (2024).
51. Wu, Y. Y. et al. Aberrantly reduced expression of mir-342-5p contributes to CCND1-associated chronic myeloid leukemia progression and imatinib resistance. *Cell. Death Dis.* **12**, 908. https://doi.org/10.1038/s41419-021-04209-2 (2021).
52. Chen, C. L. et al. Targeting S1PR1 may result in enhanced Migration of Cancer cells in bladder carcinoma. *Cancers (Basel)*. **13**, 4474. https://doi.org/10.3390/cancers13174474 (2021).

Author contributions

Conceptualization: CJL, SMH, and TWC; data curation: CJL, STL, ZSW, and TWC; formal analysis: STL and ZSW; funding acquisition: SMH and TWC; investigation: STL and ZSW; methodology: STL and ZSW; project administration: CJL; supervision: SMH; validation: STL; writing—original draft: CJL; writing—review and editing: TWC. All the authors have read and approved the final manuscript.

Funding

This work was supported by grants from the Ministry of Science and Technology [MOST 111-2320-B-016-012 to S-M Huang], the Teh-Tzer Study Group for Human Medical Research Foundation (A1111035 to S-M Huang), and the Tri-Service General Hospital [TSGH-D-11203 to T-W Chen], Taiwan, Republic of China.

Declarations

Competing interests

The authors declare no competing interests.

Additional information

Supplementary Information The online version contains supplementary material available at https://doi.org/10.1038/s41598-025-85766-w.

Correspondence and requests for materials should be addressed to T.-W.C.